ION-CHANNEL ENTRANCES INFLUENCE PERMEATION

Net Charge, Size, Shape, and Binding Considerations

JOHN A. DANI
Section of Molecular Neurobiology, Tompkins 5 Yale University School of Medicine, New Haven, Connecticut 06510

ABSTRACT Many ion channels have wide entrances that serve as transition zones to the more selective narrow region of the pore. Here some physical features of these vestibules are explored. They are considered to have a defined size, funnel shape, and net-negative charge. Ion size, ionic screening of the negatively charged residues, cation binding, and blockage of current are analyzed to determine how the vestibules influence transport. These properties are coupled to an Eyring rate theory model for the narrow length of the pore. The results include the following: (*a*) Wide vestibules allow the pore to have a short narrow region. Therefore, ions encounter a shorter length of restricted diffusion, and the channel conductance can be greater. (*b*) The potential produced by the net-negative charge in the vestibules attracts cations into the pore. Since this potential varies with electrolyte concentration, the conductance measured at low electrolyte concentrations is larger than expected from measurements at high concentrations. (*c*) Net charge inside the vestibules creates a local potential that confers some cation vs. anion, and divalent vs. monovalent selectivity. (*d*) Large cations are less effective at screening (diminishing) the net-charge potential because they cannot enter the pore as well as small cations. Therefore, at an equivalent bulk concentration the attractive negative potential is larger, which causes large cations to saturate sites in the pore at lower concentrations. (*e*) Small amounts of large or divalent cations can lead to misinterpretation of the permeation properties of a small monovalent cation.

INTRODUCTION

Since the pioneering work of Hodgkin and Huxley (1952), there has been an increasingly rapid growth in our knowledge of ion channels (see Hille, 1984 book). Biochemists have recently provided the complete amino acid sequences of the Na channel (Noda et al., 1984) and the acetylcholine receptor (Noda et al., 1983), and biophysicists have directly revealed single-channel properties with patch-clamp techniques (see Sakmann and Neher, 1983 book). The union of these two disciplines holds great promise, and is already giving unprecedented information correlating structure and function (Mishina et al., 1985; White et al., 1985).

Ion permeation models also have progressed to describe more detailed structural and electrophysiological data. Eyring rate theory and continuum approaches based on the Nernst-Planck differential equation have long provided quantitative methods for analyzing and describing ion transport. Recently, more sophisticated models have addressed physical properties of the system. Continuum modeling has been extended to examine ion interactions within the channel (Levitt, 1982). To approximate gross structures, shape has been introduced into rate-theory barriers and wells (Eisenman et al., 1985). Molecular motions of the channel have been modeled to influence ion transport via time-dependent fluctuations in the energy profile (Frehland, 1979; Lauger et al., 1980). Brownian dynamics (Cooper et al., 1985; Gates and Jakobsson, 1985) and molecular dynamics (Fischer et al., 1981; Lee and Jordan, 1984; Mackay et al., 1984) simulations have computed detailed transport properties on different time scales.

Most efforts aimed at describing permeation have focused on the narrow region of the pore, where the ion must approach the channel walls. This report, however, explores how the channel entrances may influence ion transport. Many channels have funnel-shaped vestibules that lead to the selective narrow region deeper in the pore: this includes the Na channel, the acetylcholine receptor (AChR) channel, the delayed rectifier, the sarcoplasmic reticulum K channel, and the Ca-dependent K channel (see Latorre and Miller, 1983 review, and Hille, 1984 book).

The molecular details we wish to understand are terribly complex. To get a sense of the problem consider the AChR, which roughly has an open pore that is 11 nm long (Kistler et al., 1982), the outer entrance is 2.5 nm in diameter, the inner is 1.5 nm (Brisson and Unwin, 1985), and the narrow region is 0.8 nm wide (Maeno et al., 1977; Huang et al., 1978; Dywer et al., 1980). The pore is thought to be lined by hydrophilic amino acids that include tens of negative and positive charges, but only a small net charge (Guy, 1984; Finer-Moore and Stroud, 1984; Bash et al., 1985;

Young et al., 1985). Given the large size, it is likely each vestibule contains many ions, and in the widest parts the molecular behavior is much like bulk solution. Deeper into the channel, where the vestibule narrows, the ions experience the membrane potential. (The gradient of the potential difference across the membrane becomes progressively steep as the channel narrows.) Even if the selectivity region contains only one or two ions, the adjacent vestibule contains many ions that interact more strongly as the cross-sectional area of the pore decreases. Possibly the area next to the narrow region is a multiply occupied energy minimum that does not behave like a single site. General shape considerations alone suggest a progressive shift from a bulk-like to a selectivity filter situation with the funnel-shaped vestibule serving as the transition zone.

The overall permeation process includes many factors: specific binding, local and net charge on the protein, dipoles, quadrapoles, image potentials due to the lower dielectric of the protein and lipid, molecular properties of water, ion and channel site hydration and dehydration, thermal fluctuations of the protein, excluded volume effects, and steric hinderances. Any model intended to fit experimental data with only a few adjustable parameters can only crudely approximate several of the primary factors involved. This model accounts for some physical properties of the vestibule, and then couples that to a model of the narrower region of the pore. The vestibule is considered to be in equilibrium with the bulk solution, have a net charge, and have a defined size and shape. Ion size, binding, and blocking are considered in determining how the vestibule provides a "conditioned" environment for the narrow region. Preliminary communication of this work has been made to the Society for Neuroscience (Dani, 1985).

DESCRIPTION OF THE MODEL

At least some pores have net-negative charge (Guy, 1984; Finer-Moore and Stroud, 1984) that attracts cations from solution, thus forming a diffuse ionic layer with net-positive charge. Debye-Huckel theory models this type of phenomenon for an electrolyte solution by establishing an ionic cloud of opposite charge around a central ion. Gouy-Chapman theory models an electrolyte solution near a charged interface by establishing an ionic atmosphere with excess opposite charge extending out from the interface. In all of these cases an equilibrium between thermal and electrostatic forces leads to a geometry-dependent ionic distribution. These theories are similarly constructed from a Poisson-Boltzmann equation that is derived for the specific geometry involved.

In this channel model, net-negative charge is placed on the walls of a vestibule that has a defined size and shape, and approximations are made to calculate the resulting potential as a function of position along the pore axis. A Poisson-Boltzmann equation is derived to calculate the positively charged diffuse–double-layer potential that partially counters the negative net-charge potential of the vestibule. In addition, the cations attracted into the channel can bind to the vestibule's negative residues, thus cancelling some of that net charge. Because of their size, when ions bind in the vestibule they decrease the cross-sectional area available for current carrying ions to pass through. In this model the transport rate constants are scaled by the available area to account for the blocking.

The narrow region of the channel is described by a symmetrical two-barrier, one-site (2B1S) Eyring rate theory model. This minimal model presents energy barriers to ions entering the narrow region from the wider vestibules, and provides a saturable site that prevents the channel conductance from increasing indefinitely as the ionic concentration is increased. The vestibule is considered as an equilibrium bulk phase that influences ion transport: its potential alters the driving force for transport; it determines the ionic concentrations next to the narrow region, and ion binding in the vestibule decreases the 2B1S rate constants.

THEORY

The total potential (V_t) experienced by an ion at any position is the sum of the potentials resulting from the charges on the vestibule walls (V_v), the ionic diffuse-double layer (V_d), the fraction of the applied potential felt at the given position, and all other electrostatic or chemical potentials that exist. For simplicity, all the applied potential is taken to drop across the narrow length of the channel, and only V_v and V_d are considered in the vestibule.

In reality it is likely the channel walls contain many charges distributed along the pore length. From a long distance away an ion senses only the net charge, but once inside the pore the ion experiences a variable electrostatic potential dependent upon its position and the exact distribution of charged residues. Since distances even within the vestibule are large relative to the Debye length, nearby charges are felt but distant ones are largely screened by the ionic environment. Thus, when cations are in a position to be transported they do not simply sense the net charge, rather they sense a particular value of a position-dependent local potential that fluctuates around some mean value. Since this is difficult to model and not enough information is available to determine the discrete charge distribution, the situation is approximated by placing the net charge at the inner end of the vestibule near the central narrow region. The total vestibule potential is calculated to achieve a constant value at a position 75% of the way through the vestibule near the narrow region. In this way the final potential in the vestibule that is coupled to the 2B1S model has the net vestibule charge partially screened. In addition, the image potential, that results from the lower dielectric protein surrounding the water filled pore, counters the cation concentrating effect of the net-negative charge located at the edge of the narrow region. The oppositely charged values of both the image and vestibule potentials grow as the narrow region is approached. This also supports the practice in these calculations of having the total potential achieve an average constant value before it reaches the narrow region. Unless stated otherwise, the channel is taken to have a funnel-shaped vestibule at each end that is 6.5 nm long, a 2.6 nm diam facing the bulk solution, and a 1.2 nm diam next to the narrow region.

Potential Due to the Net Charge in the Vestibule (V_v)

In this treatment an approximation is made that half the field lines due to the charged residues proceed down the pore and exit into the bulk solution. The other half enters the protein or is cancelled by the field lines

from the other vestibule due to symmetry. If the dielectric constant of the pore water were infinitely higher than the surrounding dielectric, then all the field lines would be confined to the pore (Levitt, 1985). The factor of 0.5 accounts, in part, for the nonzero dielectric constant of the channel protein.[1] In addition, the field is crudely considered not directly to affect the 2B1S model. In a perfectly symmetrical channel the field from the two vestibules would cancel in the narrow region, and in other situations the energies of the barriers and site could be adjusted to partially account for the field's influence.

The field from the net charge (N) in the vestibule is calculated from Gauss's Law:

$$E_v = \frac{1}{2}\frac{4\pi Ne}{\epsilon A(x)}, \tag{1}$$

where the 1/2 accounts for only half the field lines being effective as explained above, e is elementary charge, ϵ is the dielectric constant of water, and $A(x)$ is the surface area perpendicular to the field lines at position x along the channel axis. This surface area of constant, uniform electric field is approximately given by:

$$A(x) = \begin{cases} \pi r^2 & 0 < x < L \\ \pi(R^2 + (x - L)^2) & L \le x < L + R \\ 2\pi (x - L)^2 & L + R \le x, \end{cases} \tag{2}$$

where L is the length of the vestibule, R is the radius of the vestibule at its opening to the bulk solution, and r is the radius of the vestibule at x. Fig. 1 schematically represents the pore geometry, the electric field lines, and the constant field surfaces.

The potential that results from the charges in the vestibule is (Levitt, 1985)

$$V_v = -\int E_v \, dx = -\frac{1}{2}\frac{4\pi Ne}{\epsilon}\int_\infty^x \frac{dx}{A(x)}. \tag{3}$$

To perform the numerical integration that calculates the diffuse–double-layer potential (V_d), it is necessary to set a practical position where V_v becomes insignificant and does not influence the electrolyte solution. This position can be set by assuming there is mixing in the bulk solution at a long distance from the channel. The distance was taken as the length of the vestibule plus 1.5 times the widest radius of the channel plus two Debye lengths. This is more than sufficient because the total vestibule potential (V_t) falls more rapidly than predicted by the Debye length from Gouy-Chapman theory. This location also serves as the $x = \infty$ boundary condition for calculating V_d.

Diffuse–Double-Layer Potential (Vd)

The diffuse–double-layer potential results from the excess positive electrolyte charge attracted by the oppositely charged residues in the vestibule. Derivation of the relevant Poisson-Boltzmann equation follows from Gauss's Law (Levitt, 1985), given that the field from the excess diffuse charge remains primarily in the pore. This is the same approximation used for the field that arises from the net charge in the vestibule. It is reasonable because the dielectric constant of the pore water is substantially greater than the surrounding protein and lipid. In addition, the error introduced by this approximation is diminished because it is applied to two fields of opposite sign.

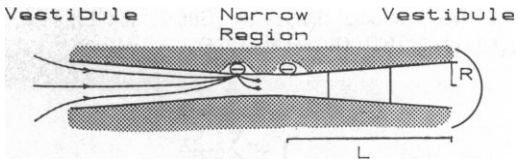

FIGURE 1 A schematic representation of the symmetrical channel geometry. The electric field lines are represented in the left vestibule. The field lines in the narrow region are canceled by the field lines from the right vestibule (not shown). The single net charge at the end of each vestibule is represented by a large minus that is drawn out of scale. The solid lines and the half circle in the right vestibule represent the cross-sectional areas $A(x)$, with the line nearest the narrow region marking the place where the numerical integration ends. L is the length of the vestibule, and R is the radius of the opening to the bulk solution.

The field lines pass down the pore perpendicular to the same uniform constant-field surfaces given in Eq. 2. Gauss's Law gives

$$\oint E \, dA = E_d(x)A(x) = 4\pi q/\epsilon, \tag{4}$$

where q is the net electrolyte charge enclosed in the Gaussian surface extending from 0 (where the vestibule's net charge is located, next to the narrow region) to x, and E_d is the electric field from the diffuse charge. The spatial variation in the diffuse–double-layer potential results from the distribution of the ionic atmosphere that is used to calculate q. The charge in a volume element $A(x)dx$ at x is given by the sum of all the ions in that volume element:

$$q(x) = \sum_j z_j e C_j A_j(x) \, dx, \tag{5}$$

where j is the ion species, zj is the ion valence, C_j is its concentration in the volume element, and A_j is the effective cross-sectional area available for the center of the ion. For large ions $A_j(x)$ is much smaller than the cross-sectional area of the channel $A(x)$. The total charge in the diffuse–double-layer is the sum of the charges in each element:

$$q = \int_0^\infty q(x) \, dx = \int_0^\infty \sum_j z_j e C_j A_j(x) \, dx. \tag{6}$$

By definition $Ed(x) = -dV_d/dx$, which along with Eqs. 4 and 6 gives

$$-A(x)\frac{dV_d}{dx} = \frac{4\pi}{\epsilon}\int_0^\infty \sum_j z_j e C_j A_j(x) \, dx. \tag{7}$$

The Boltzmann equation introduces the equilibrium dependence of the local concentration (C) on the bulk concentration (C_b) and the total potential ($V_t = V_v + V_d$):

$$C_j = C_{bj} \exp\left(\frac{-z_j F V_t}{RT}\right). \tag{8}$$

Differentiating both sides of Eq. 7 by x and substituting in Eq. 8 gives the final Poisson-Boltzmann equation containing the diffuse–double-layer potential (V_d):

$$\frac{d}{dx}\left(A(x)\frac{dV_d}{dx}\right) = -\frac{4\pi e}{\epsilon}\sum_j z_j A_j(x) C_{bj} \exp\left(\frac{-z_j F V_t}{RT}\right). \tag{9}$$

Binding to the Vestibule's Net Charge

Cations attracted into the channel by the negatively charged protein residues can bind and reduce the number of free charges contributing to V_v. For monovalent cations conventional equilibrium binding gives the

[1]The best choice for this factor will depend on the pore geometry and the dielectric properties of the system. The choice of 1/2 is a reasonable compromise for a general calculation. In addition, the significance of the model is in the qualitative properties it reveals not the precise values of the potentials it produces. Another method that is often used to account for the dielectric constant of the channel is to make the effective high dielectric diameter of the pore larger than its physical size (see Jordan, 1984).

number of free vestibule charges as (Gilbert and Ehrenstein, 1969; McLaughlin et al., 1971; Hille et al., 1975)

$$N_f = \frac{N}{1 + \sum_j \frac{C_j}{K_{dj}}}, \quad (10)$$

where N is the number of net charges in the vestibule, C_j is the concentration in the vestibule, and K_{dj} is the equilibrium dissociation constant of species j. In practice an iterative algorithm calculates the amount of each species bound. In this way the size and charge of each species can be used to determine blockage and the final net charge of the channel.

Due to the finite size of the ions, cation binding to the net charge reduces the cross-sectional area next to the narrow region of the pore that is available to pass current. This is introduced into the model by reducing the 2B1S rate constants by a factor related to the available cross-sectional area:

$$k_e = K_v k$$

$$K_v = 1 - \sum_j \frac{N_{bj} R_{cj}^2}{R_x^2}, \quad (11)$$

where ke is the effective rate constant after binding, k is the rate constant without binding, N_{bj} is the number of species j bound, R_{cj} is the radius of the cation, and Rx is the radius of the pore at the position where binding occurs. In these calculations binding occurs at a position 75% of the way through the vestibule nearing the narrow central region. Except for the specific size dependence, the same results are obtained for binding at other positions.

2B1S Rate Theory Model in the Narrow Region

The narrow region of a channel is critical for transport, and most permeation models rightly focus on this region to describe selectivity and other transport properties. In this paper a symmetrical two-barrier, one-site (2B1S) model provides the minimal requirements expected from the narrow length of the channel. Fig. 2 shows a symmetrical 2B1S energy profile with the rate constants labeled for two ion species (1, 2) over two barriers (o, i) in the inward or outward (−) direction. Rate constants for ion jumps from the vestibules to the site are defined as

$$k_v = K_v K_t \frac{bT}{h} \bar{V}_w \exp - \frac{G_v}{RT} \exp \frac{-D_v z F V_e}{RT}, \quad [\mathrm{Ms}]$$

and for jumps from the site to the vestibules as

$$k_v = K_v K_t \frac{bT}{h} \exp - \frac{G_s}{RT} \exp \frac{-D_s z F V_e}{RT}, \quad [\mathrm{s}],$$

where K_v is the factor that reduces the rate constant dependent on the available cross-sectional area (Eq. 11); K_t is the transmission coefficient, which is taken as unity; bT/h is the molecular vibration frequency[2] taken as $6.12 \times 10^{12}\ s^{-1}$; G_v is the free energy difference between the vestibule and the top of the appropriate barrier; G_s is the free energy difference between the site and the top of the appropriate barrier; D_v and D_s are the corresponding fractional electrical distances; V_w is the molar volume of water taken as its bulk value of $1.80 \times 10^{-3}\ L/M$; b is the Boltzmann constant; and the other constants have their usual values. The electrical

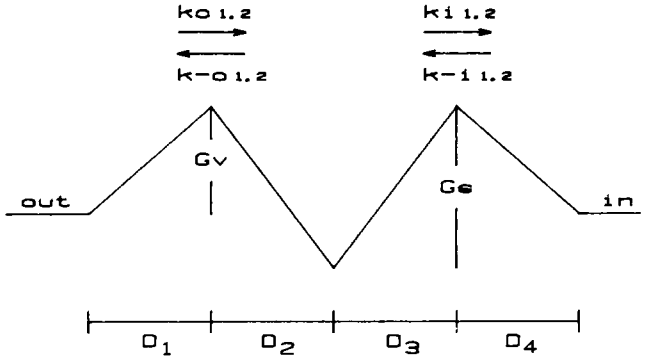

FIGURE 2 A symmetrical 2B1S energy profile where the k's are rate constants for transitions over the outer (o) or inner (i) barrier by cation species 1 or 2 in the inward or outward (−) direction; G_s is the free energy change for ion jumps out of the site; G_v is for ion jumps from the vestibules into the site; the D's are fractional electrical distances. For the main permeant (1) the barriers are 8 KT and the site −4 KT, and for the secondary permeant (2) the values are 10 KT and −5 KT unless stated otherwise. Inward going current is defined as negative.

distances in Fig. 2 determine the fraction of the effective potential that is experienced by an ion during a jump. For simplicity, all the effective voltage falls across the narrow region of the channel, giving $D_1 + D_2 + D_3 + D_4 = 1$.[3] In addition, the barrier model is symmetrical, giving $D_1 = D_2 = D_3 = D_4 = 0.25$. The effective voltage drop (V_e) across the 2B1S portion of the model channel results from the applied potential (V_a) and the difference in the total vestibule potentials: $V_e = V_a + V_{ti} - V_{to}$.

In the presence of two permeant species, standard Eyring rate theory (Lewis and Stevens, 1979; Hagglund et al., 1984) gives the steady state probability for the central site being empty:

$$P_e = (k_{i1}k_{i2} + k_{i2}k_{-o1} + k_{i1}k_{-o2} + k_{-o1}k_{-o2})/\mathrm{Denom}$$

occupied by species 1:

$$P_1 = (C_{i1}k_{-i1}k_{i2} + C_{i1}k_{-i1}k_{-o2} + C_{o1}k_{o1}k_{i2} + C_{o1}k_{o1}k_{-o2})/\mathrm{Denom}$$

or occupied by species 2:

$$P_2 = (C_{i2}k_{-i2}k_{i1} + C_{i2}k_{-i2}k_{-o1} + C_{o2}k_{o2}k_{i1} + C_{o2}k_{o2}k_{-o1})/\mathrm{Denom}$$

$$\mathrm{Denom} = C_{i1}(k_{-i1}k_{-o2} + k_{-i1}k_{i2}) + C_{o1}(k_{o1}k_{-o2} + k_{o1}k_{i2}) + C_{i2}(k_{-i2}k_{i1} + k_{-i2}k_{-o1}) + C_{o2}(k_{o2}k_{-o1} + k_{o2}k_{i1}) + k_{i1}k_{i2} + k_{i2}k_{-o1} + k_{i1}k_{-o2} + k_{-o1}k_{-o2}$$

and $P_e + P_1 + P_2 = 1$. The C's are concentrations in the vestibules, which are related to the bulk concentrations by an equilibrium Boltzmann factor of the total vestibule potential: $C = C_b \exp -(zFV_t/RT)$.

The steady state current is the same over either barrier, and is equal to the difference in the one-way fluxes. The steady state current calculated

[2]This is the most commonly used value of the frequency factor. Its value does not change the meaning of the results, but the currents produced from the energy profile are scaled by this term.

[3]In reality some voltage drop is expected in the vestibules, with the actual value dependent on the exact properties of the pore and the bathing solution. Introducing this complication would change the exact energy profiles for permeation but not the general transport characteristics revealed by this model.

over the outer barrier, with inward current defined as negative is

$$I = e(z_1 P_1 k_{-o1} + z_2 P_2 k_{-o2} - z_1 C_{o1} P_e k_{o1} - z_2 C_{o2} P_e k_{o2}). \quad (12)$$

METHODS

Theoretical currents are produced by calculating the properties of the vestibules and then using those results in the 2B1S portion of the model. The principle problem is to determine the diffuse potential (V_d) by numerically solving the nonlinear two-point-boundary problem in Eq. 9. The boundary conditions are that $V_d = 0.0$ at a long distance from the channel where the solution is well stirred, and at a position well into the channel V_d stops changing ($dV_d/dx = V_{d'} = 0.0$). In practice, mixing occurs ($V_d = 0.0$) and the concentrations equal their bulk values at a distance (referred to as X_{init}) equal to the length of the vestibule plus 1.5 times the largest radius of the channel plus two Gouy-Chapman defined Debye lengths. The first derivative of the diffuse potential equals zero at a position 75% of the way through the vestibule (X_{fin}) near the center of the channel.

Eq. 9 is numerically integrated for V_d using the "shooting method" (see Acton, 1970 book). A guess is made for $V_{d'}$ at X_{init} and the equation is integrated to X_{fin}. If $V_{d'}$ at X_{fin} is not equal to zero (0 to -0.5 is accepted), another $V_{d'}$ at X_{init} is guessed and the procedure is repeated until the boundary condition is met. A "bisection method" is used to update the guess.[4] The correct value of $V_{d'}$ at X_{init} falls within an initially set liberal range. After each iteration the range is made smaller by setting the appropriate limit of the range equal to the $V_{d'}$ guess that just failed. The next guess is equal to a value in the middle of the new range. Each iteration cuts the range in half. Although this procedure is not fast, it always converges to the correct $V_{d'}$ if the calculation has enough precision.

The actual numerical integration is begun using a fourth order Runge-Kutta method. This method is slow but it requires no previous information; so it is ideal for accurately calculating the first three steps in the marching process. Milne's predictor-corrector method uses these initial three points and proceeds more rapidly through the rest of the integration. For each step all the values that depend on x, such as the cross-sectional area and V_w, are calculated and used to determine V_d and finally the total potential (V_t) at that position. The final step size used in the marching process was selected by making the step size progressively smaller until the answer was unchanged.

Cation binding to the net-negative charge in the vestibule takes place by an iterative process. Initially the vestibule has an assigned number of charged sites ($N = N1$). After the integration converges, the total potential (V_t) and the ion concentrations in the vestibule are known for $N1$. Ions then bind to the net charge in the vestibule (see Eq. 10) reducing the number of free charged sites ($N2 < N1$). The integration is repeated to determine V_t with $N = N2$. Since there are fewer free negative charges, less cations are attracted into the channel and therefore less binding occurs ($N2 < N3 < N1$). This continues until N changes by <5% in a binding iteration. In practice the binding actually converges faster than just described because a job-specific "bisection" algorithm achieves the final N with fewer iterations.

When only one monovalent cation species can bind, Eqs. 10 and 11 directly give the influence of cation size on transport. When two different sized ions bind, an iterative procedure determines the number of each specie bound. Then the area occluded by the overall binding and the effect on the 2B1S rate constants is determined as usual. When a divalent cation binds, it eliminates two negative charges, but it blocks the channel dependent only on its cross-sectional area like any other cation.

The programs are written in double-precision Fortran IV, and they were run on PDP 11-23 and PDP 11-73 computers (Indec Systems Inc., Sunnyvale, CA) using RT-11 as the operating system.

[4] I thank Dr. C. Clausen for suggesting this method.

RESULTS AND DISCUSSION

Comparison with Gouy-Chapman Theory

Gouy-Chapman theory approximates a charged surface as an infinite, structureless, impenetrable plane with a uniformly smeared charged density. The charge density (σ) is given by (Grahame, 1947)

$$\sigma = \left(2\epsilon_r\epsilon_o N_n bT \sum_j C_{bj} \exp\left(\frac{z_j e V_{surf}}{bT}\right) - 1\right)^{1/2},$$

where ϵ_r is the dielectric constant, ϵ_o is the permittivity of free space, N_n is Avogadro's number, C_{bj} is the bulk concentration of species j, and V_{surf} is the surface potential.

Fig. 3 *A* illustrates the parallel field lines eminating from a uniformly charged plane and the diverging field lines associated with the funnel-shaped entrance of a channel. The field lines spread out to uniformly occupy the vestibule; then they diverge dramatically as they enter the bulk solution where they are no longer confined by the lower dielectric of the protein. The Gouy-Chapman field lines, however, remain parallel and constant from the plane surface to infinity. Therefore, in an infinitely dilute solution that does not have an ionic double layer, the planar field interacts equally with an ion located at infinity or near the surface. In contrast, an ion experiences a stronger force as it approaches the concentrated field lines near or in a charged channel vestibule. Thus, there are qualitative

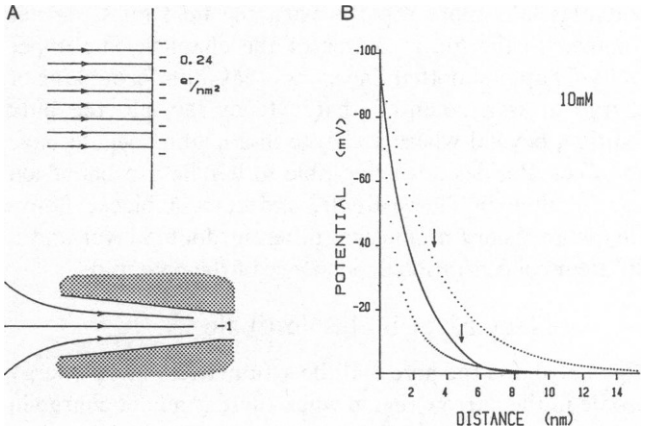

FIGURE 3 (*A*) The parallel field lines associated with a uniformly charged plane are constant from the surface of the plane to infinity. The field lines associated with a funnel-shaped vestibule diverge as they pass into the bulk solution. (*B*) The spatial distribution of the total potential in 10 mM monovalent electrolyte was calculated from the charged-vestibule theory with $N = -1$ and $K_d = \infty$ (solid line). The $x = 0.0$ position corresponds to the position in the vestibule where the numerical integration ends. The value of the potential there is $V_t = -95.8$ mV. The arrow at 4.9 nm labels where the channel opens to the bulk solution. The upper dotted line was calculated from Gouy-Chapman theory with a surface potential at $x = 0.0$ set equal to -95.8 mV. The arrow at 3.2 nm labels the Debye length. The lower dotted line was obtained by dividing the Gouy-Chapman potential by $(1 + x)$ to approximate how the potential falls off from a -95.8 mV initial point in bulk solution.

differences in the spatial distribution of the ionic double layers that develop.

Fig. 3 *B* shows how the total potential falls off with distance in 10 mM monovalent electrolyte. The solid line represents the charged-vestibule theory with 0.0 nm corresponding to the place where the numerical integration stops, 75% of the way through the vestibule. The potential at that position is $V_t = -95.8$ mV, and the arrow at 4.9 nm marks where the vestibule opens to the bulk solution. The upper dotted line represents the small potential approximation of Gouy-Chapman theory obtained from (see McLaughlin, 1977 review)

$$V_{gc} = V_{surf} \exp(-\kappa x)$$

$$K = \left(\frac{2e^2 C_b N_n z^2}{\epsilon_r \epsilon_o bT}\right)^{1/2},$$

where the potential (V_{gc}) falls to 1/2.72 its surface value (V_{surf}) at a distance equal to the Debye length ($1/\kappa$), which is marked by an arrow at 3.2 nm. The Gouy-Chapman surface potential was set equal to −95.8 mV to match that obtained with the charged-vestibule theory. This V_{surf} corresponds to a uniform charge density of 0.24 charges/nm^2 in 10 mM electrolyte. The lower dotted line is given by $V_{gc}/(1 + x)$, where x is distance. This represents how the potential would decrease with distance from a reference point if the field lines spread out with spherical symmetry.

This figure indicates that simpler approaches based on Gouy-Chapman theory could not adequately replace the charged vestibule theory. The lower dotted line shows the potential falls more rapidly when the field lines are not confined to the finite volume of the channel. The upper Gouy-Chapman dotted line shows that a uniform plane of charge gives a potential that extends far into the bulk solution, beyond where a charge in a channel would have an effect. Besides not being able to handle aspects of ion size, binding in the vestibule, and current block, Gouy-Chapman theory produces a different double layer and a different concentration dependence of the potential.

Net Charge in the Vestibule

Fig. 4 *A* shows the pore and the symmetrical 2B1S energy profile in the narrow region when there is no net charge in the vestibule. Zero free energy is defined in bulk solution and extends to the beginning of the narrow region because the vestibules are approximated as being in equilibrium with the bulk solution. In this model the width of the narrow region does not enter into the calculation; so the shape of the channel where the vestibule and narrow region meet could be much different. Ion transport in this case depends only on the 8 KT barriers and the −4 KT site. The bottom of the figure displays the current-voltage (*I-V*) relations that result in 1, 150, and 1,000 mM electrolyte. In 1 mM solution the current per channel is almost undetectable, while in 1,000 mM it grows to 21 pA at 200 mV. Fig. 4 *B* shows an equivalent schematic in 150 mM electrolyte

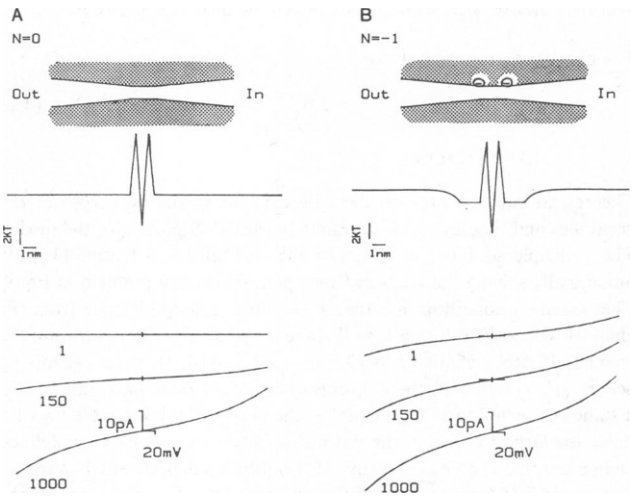

FIGURE 4 (*A*) The pore, the symmetrical 2B1S energy profile, and the *I-V* relations in 1, 150, and 1,000 mM monovalent electrolyte for a channel that has 8 *KT* barriers, a −4 *KT* site, and no net charge ($N = 0$). (*B*) The same schematic when $N = -1$, $K_d = \infty$, and the radius of the permeant cation is $R_c = 0.095$ nm. For simplicity, the net charge in each vestibule is represented by a large minus that is drawn out of scale. The charge in the vestibule and the energy barriers and well in the narrow region could result from distributed rings of positive and negative residues not represented here. The energy profile was calculated in 150 mM electrolyte, and the final value of the vestibule potential is $Vt = -42$ mV. This concentration-dependent negative potential results in the channel passing significant current even at low electrolyte concentrations.

when each vestibule contains −1 net charge. The energy profile dips down in each vestibule and then maintains a final constant value for the most central 25% of the vestibule. The diffuse potential (V_d) varies with concentration, thereby causing the vestibule's total potential (V_t) to be more negative at low concentrations. This negative potential attracts cations into the channel; so there is significant current even in 1 mM electrolyte, as seen in the bottom of Fig. 4 *B*.

Fig. 5 shows how V_t varies as a function of the vestibule's net charge (N) at various electrolyte concentrations. The attractive negative potential is larger at more negative N and at low bulk electrolyte concentrations. Therefore, relative to the bulk concentration (C_b) the vestibule concentration (C_v) is greater; so more cations are in a position to pass through the channel: $C_v/C_b = \exp(-zV_t/25.35)$. This feature leads to higher conductances at low concentrations than predicted from conductances measured at high concentrations (also see the *I-V* relations in Fig. 4 *B*).

The net charge also can produce simple selectivity. For example, in a bulk solution of 150 mM NaCl plus 10 mM $CaCl_2$ with a net vestibule charge of $N = -1$ and no binding to that charge, the total vestibule potential predicted by the model is $V_t = -37$ mV. That increases the Ca^{++} concentration in the vestibule by a factor of 18.0 and decreases the Cl^- concentration by a factor of 4.2 relative to their bulk concentrations. The negative potential in the vestibule selects for cations over anions, and divalents over

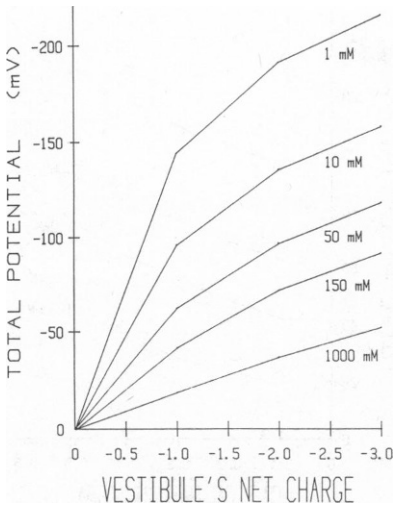

FIGURE 5 The total vestibule potential (V_t) plotted vs. the vestibule's net charge (N) with the monovalent electrolyte concentration equal to 1, 10, 50, 150, or 1,000 mM, and $K_d = \infty$, $R_c = 0.095$ nm. As the electrolyte concentration is decreased, there is less screening and V_t becomes more negative.

monovalents. Besides the general potential described in this treatment, it is possible that stronger local potentials contribute to this selectivity before the final "selectivity filter" in the narrow region.

Binding to the Vestibule's Net Charge

Fig. 6 schematically shows how the potentials vary in going from a 150 mM bulk solution to the place where the numerical iteration stops. Fig. 6 *A* has $N = -1$, no binding to that charge ($K_d = \infty$), and has a final $V_t = -42$ mV. It can be seen that the diffuse potential (V_d) counters most of the vestibule's net-charge potential (V_v) and the total potential ($V_t = V_v + V_d$) is smaller than both of its components. When cations bind to the charge with $K_d = 50$ mM, Fig. 6 *B* shows that the absolute values of all the potentials decrease because the number of free charges falls to $N_f = -0.21$ giving a final $V_t = -6$ mV.[5]

Fig. 7 shows how V_t varies when there is binding to the net charge. The *X* next to the curve at each concentration is the value of V_t if there were no binding ($K_d = \infty$). As the electrolyte concentration increases, the *X*'s illustrate how increased screening of the charge decreases the absolute value of V_t. This results because V_v remains constant while V_d becomes more positive with increasing concentration. The effect of binding is to decrease the number of free negative charges. As K_d decreases, binding increases: N_f and V_v become smaller negative numbers and therefore so does V_t.

[5]Equilibrium binding effectively produces a fraction of a free charge ($N_f = -0.21$) as a result of rapid binding and unbinding of the cation to the negatively charged site. In this case the negative charge is free 21% of the time.

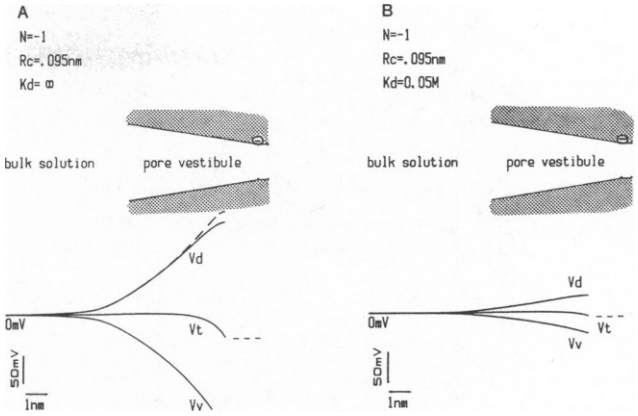

FIGURE 6 Schematic drawing of the vestibule facing into a bulk solution of 150 mM monovalent electrolyte. The values of the potentials at the corresponding positions along the pore axis are drawn underneath the vestibule: V_v is the vestibule's net-charge potential, V_d is the diffuse-double-layer potential, and V_t is the total potential ($V_t = V_v + V_d$). The potentials fall to 0 in the bulk solution. The dashed line next to each V_t curve signifies that the total potential remains constant for the last 25% of the vestibule length near the narrow region. (*A*) In this case $N = -1$, $R_c = 0.095$ nm, and $K_d = \infty$. The dashed V_d curve is the diffuse-double-layer potential that would develop if the cation in solution were a divalent. (*B*) In this case $N = -1$, $R_c = 0.095$ nm, and $K_d = 50$ mM. Cation binding to the negative net charge reduces the absolute values of all the potentials.

Fig. 8 indicates how binding to the net charge masks its influence on transport and can lead to the misinterpretation of data. Fig. 8 plots conductance (G) vs. concentration (C) for $N = -1$ with no binding (∇), with $K_d = 50$ mM (+), and the dotted Michaelis-Menten curve is for $N = 0$ (see Fig. 4 *A*). When there is significant binding, it is hard to tell the difference between the case with net charge and

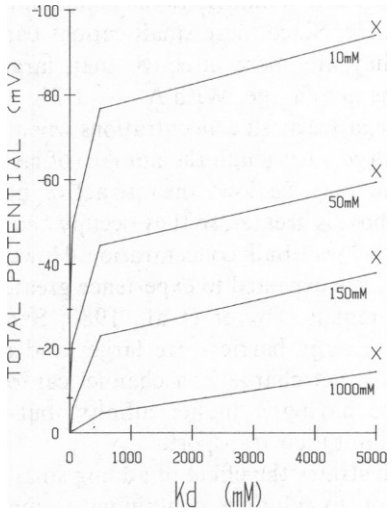

FIGURE 7 The total vestibule potential (V_t) plotted vs. the dissociation constant (K_d) for binding to the vestibule's net charge ($N = -1$) in various bulk concentrations of monovalent electrolyte. The *X*'s next to each curve represent V_t when there is no binding ($K_d = \infty$) to the net charge. Values were calculated at $K_d = 5$, 50, 500, 5,000 mM, and those points are connected by straight lines. As K_d decreases, cation binding to the negative residue increases; so V_t becomes less negative.

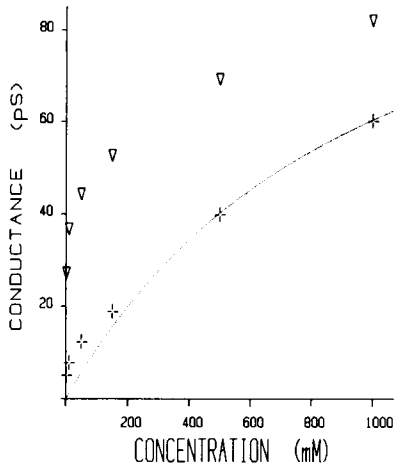

FIGURE 8 Single-channel conductance at 40 mV plotted vs. monovalent electrolyte concentration when $N = -1$, $R_c = 0.095$ nm, and $K_d = \infty$ (▽) or 50 mM (+). The dotted Michaelis-Menten curve has $G_{max} = 121.9$ pS and has a dissociation constant to the 2B1S site of $K_{site} = 1.02$ M, consistent with Fig. 4 *A*, and in all cases the 2B1S barriers are 8 KT and the site -4 KT. The general agreement between the dotted curve ($N = 0$) and the + symbols ($N = -1$, $K_d = 50$ mM) indicates that different physical descriptions of the channel can produce similar ion transport results.

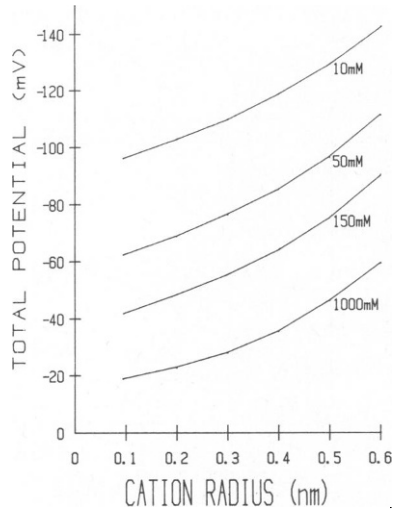

FIGURE 9 The total vestibule potential (V_t) plotted vs. the radius of the monovalent cation in solution at various concentrations for $N = -1$ and $K_d = \infty$. Values were calculated at $R_c = 0.095$, 0.2, 0.3, 0.4, 0.5, and 0.6 nm, and the points are connected by straight lines. Large cations cannot screen the negative residues as well as small cations; so V_t becomes more negative as R_c increases.

$N = 0$. In practice, detection of the net charge becomes difficult because measurements have to be made at very low concentrations where conductances are small and harder to measure. The dotted curve in Fig. 8 illustrates how a model can fit limited data well, but not accurately describe the physical properties of the channel.

Cation Size

The size of the cation influences the potential that develops in the vestibule. Since more small cations can fit into the vestibule, they are more effective than large cations at screening the net charge. With $N = -1$ Fig. 9 shows that V_t is more negative at all concentrations when the cation in solution is larger. Although the number of large cations in the vestibule may be low, the attractive potential (V_t) exerted on those is greater; so they occupy and saturate the 2B1S site at a lower bulk concentration. However, because large cations are expected to experience greater friction in the narrow region (Dwyer et al., 1980; Sanchez et al., 1986), their energy barriers are larger and their G_{max} is smaller. Thus, net charge in a channel can contribute to large cations having a higher affinity, but the narrow region may limit their transport.

Fig. 10 illustrates the effect of adding small amounts of a large cation to solutions containing a small permeant when the net charge in the vestibule is $N = -1$. Fig. 10 plots conductance (G) vs. concentration (C_1) for a small cation that does not bind to the vestibule charge ($K_{d1} = \infty$) and has a radius (R_{c1}) equal to 0.095 nm; 10 mM (▽) or 1 mM (Δ) of a large cation is always present having $K_{d2} = 5$ mM and $R_{c2} = 0.5$ nm. The solid Michaelis-Menten curves can fit the data well with apparent G_{max} and K_{site} values for the small permeant that depend on the concentration and vestibule binding of the large cation. Thus, a simple curve can fit any set of these data when N is incorrectly assumed to be zero and incorrect values of K_{site} and G_{max} are used for the small permeant. For comparison, the dotted Michaelis-

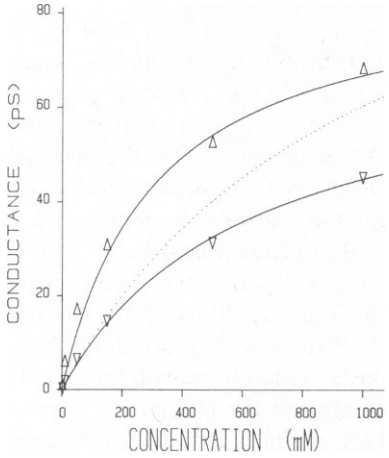

FIGURE 10 Single-channel conductance at 40 mV plotted vs. monovalent electrolyte concentration (C_1) when $N = -1$, $R_{c1} = 0.095$ nm, $K_{d1} = \infty$, and this cation encounters 8 KT barriers and a -4 KT site. The secondary cation has $R_{c2} = 0.5$ nm and $K_{d2} = 5$ mM. When the secondary cation is always present at $C_2 = 1$ mM (Δ), a Michaelis-Menten (M-M) curve with $G_{max} = 87.3$ pS and $K_{site} = 305$ mM passes near the points. When $C_2 = 10$ mM (▽), a M-M curve with $G_{max} = 72.5$ pS and $K_{site} = 615$ mM passes near the points. Thus, the transport results for the main permeant are influenced by low concentrations of a large cation. For comparison, the dotted M-M curve has $G_{max} = 121.9$ pS and $K_{site} = 1.02$ M, consistent with Fig. 4 *A*.

Menten curve is shown. It has $N = 0$ in a pure solution of the small cation (see Fig. 4 *A*).

Cation Charge

Fig. 11 shows how V_t varies as a function of the cation valence at three electrolyte concentrations when $N = -1$. As the valence of the cation is increased the vestibule potential is more effectively screened and V_t becomes smaller. The upper, dashed line in Fig. 6 *A* shows how V_d increases for a divalent cation.

With $N = -1$ Fig. 12 illustrates the effect of adding small amounts of a divalent cation to solutions of a monovalent permeant. Fig. 12 plots G vs. monovalent cation concentration C_1 with the divalent having $K_{d2} = 50$ mM and $C_2 = 1$ mM (Δ) or 10 mM (▽). Again for comparison, the dotted Michaelis-Menten curve in the figure represents $N = 0$, $G_{max} = 121.9$ pS, and $K_{site} = 1.02$ M as depicted in Fig. 4 *A*. The solid curves fit each set of data well by incorrectly assuming $N = 0$ and different apparent G_{max} and K_{site} for the monovalent cation. Therefore, a small amount of divalent cations can influence the interpretation of transport data, possibly leading to incorrect assumptions about the permeation process and the wrong values for G_{max} and K_{site}.

Channel Size and Asymmetry

Fig. 13 shows how the potentials depend on the size and shape of the vestibules. Two factors contribute to the larger potentials in the narrow vestibule: the field lines are confined to a smaller pore width, and the size of the cations make them less effective at entering the narrow pore to screen the net charge. The wider vestibule in Fig. 13 *B* allows the field lines to spread out; thus, at any position V_v is less negative. Also, in this large vestibule cations interact less sterically; so they enter the channel to produce a V_d that more completely counters V_v, which causes the absolute value of V_t to be smaller. These size and shape considerations also can affect transport. With the same net charge, various shapes would produce different potentials that could affect the selectivity, channel blockage, and apparent binding constants in the vestibules and narrow region.

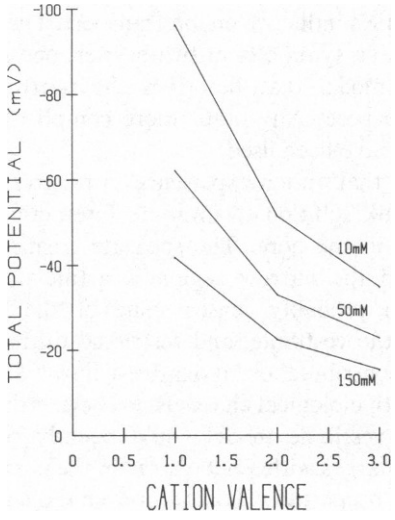

FIGURE 11 A plot of the total vestibule potential (V_t) vs. cation valence at 10, 50, and 150 mM electrolyte with $R_c = 0.095$ nm. Straight lines connect values at valences of 1, 2, and 3. As the cation valence increases, the negative residues are more effectively screened, and V_t becomes less negative.

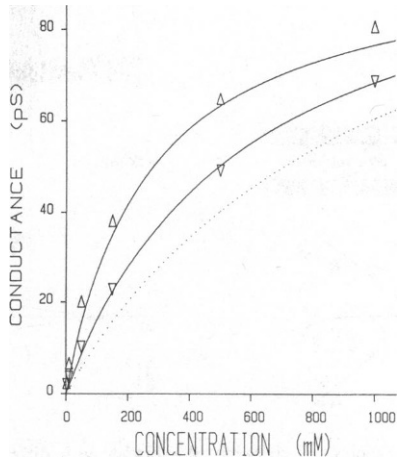

FIGURE 12 The parameters for the main, monovalent cation (C_1) are $N = -1$, $R_{c1} = 0.095$ nm, $K_{d1} = \infty$, and this cation encounters 8 KT barriers and a -4 KT site. The dotted curve is consistent with Fig. 4 *A*, having $G_{max} = 121.9$ pS and $K_{site} = 1.02$ M. The single-channel conductance at 40 mV is plotted vs. concentration (C_1) when the secondary cation is a divalent with $R_{c2} = 0.095$ nm and $K_{d2} = 50$ mM. When the divalent is always present at $C_2 = 1$ mM (Δ), a M-M curve with $G_{max} = 97.0$ pS and $K_{site} = 265$ mM passes near the points-. When $C_2 = 10$ mM (▽), a M-M curve with $G_{max} = 107.9$ pS and $K_{site} = 575$ mM passes near the points. Thus, the transport results for the main permeant are influenced by low concentrations of a divalent cation.

Fig. 14 shows the asymmetric transport properties that result when the outer vestibule contains a net negative charge but the inner vestibule does not. Fig. 14 *A* shows the energy profile and plots conductance vs. the applied potential in 150 mM and 10 mM electrolyte. At these concentrations the inward going current is greater than the outward going current because the negative charge in the outer vestibule concentrates cations in a position for them to be transported inward. Fig. 14 *B* plots conductance (G) vs. concentration (C) at -200 mV (□) and $+200$ mV (X). At all but 1,000 mM the inward going currents (□) are larger. This demonstrates that the vestibule charge can contribute complex transport asymmetry to an otherwise symmetric channel. This cross over in the G vs. C plot at 1,000 mM is probably due to the 2B1S site starting to become saturated at this high concentration. The current then becomes limited by exit from the site. The energy profile (top Fig. 14 *A*) shows that inward going cations (exiting from the site to the right) encounter a larger barrier than outward going cations (exiting from the site to the left); so at very high concentrations outward current is favored. Qualita-

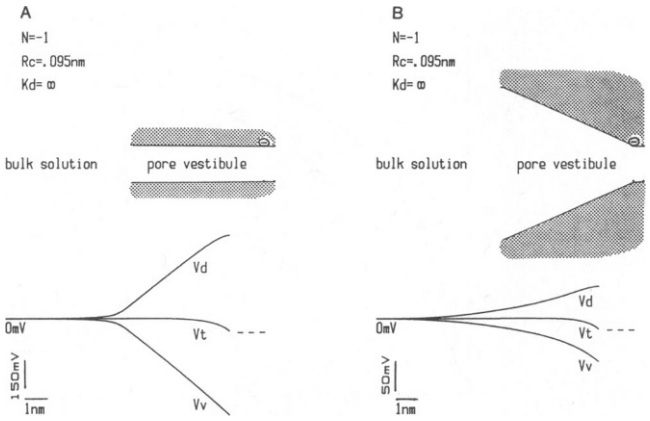

FIGURE 13 A schematic drawing like Fig. 6 with differently shaped vestibules. The vestibule's net-charge potential (V_v), the diffuse-double-layer potential (V_d), and the total potential ($V_t = V_v + V_d$) are drawn with their corresponding values along the pore axis. The potentials fall to zero in the bulk solution, and the dashed line next to the V_t curves signifies that V_t remains constant for the last 25% of the vestibule length near the narrow region. In both cases $N = -1$, $R_c = 0.095$ nm, $K_d = \infty$, and the vestibule is 6.5 nm long. The vestibule opens to the bulk solution with a diameter of 1.3 nm in *A* and 5.2 nm in *B*, and in both cases it narrows to 1.2 nm. The potential scale is compressed threefold in *A*.

tively identical results have been seen experimentally with asymmetric gramicidin channels formed with net negative charge at one end but not the other (Apell et al., 1977).

Fig. 15 illustrates transport when both the outer and inner vestibules contain one negative charge, but asymmetry is produced by cations binding to the outer vestibule but not to the inner. Fig. 15 *A* shows the energy profile and the asymmetric conductance at 150 mM and 10 mM electrolyte. Fig. 15 *B* plots *G* vs. *C* at −200 mV (□) and +200 mV (*X*). At low concentrations the channel outwardly rectifies and at 1,000 mM there is inward rectification.

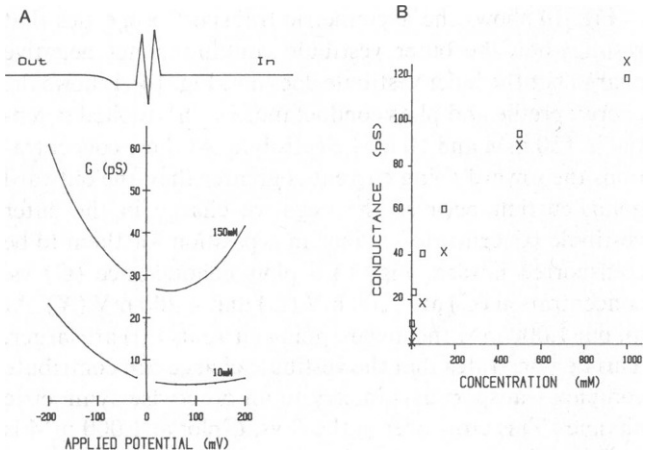

FIGURE 14 Shows asymmetric ion transport through a channel with net charge in the outer vestibule only ($N_o = -1$, $N_i = 0$). (*A*) The energy profile calculated in 150 mM electrolyte has the final, outer-vestibule potential $V_{to} = -42$ mV. Below, the single-channel conductance is plotted vs. the applied potential in 150 mM and 10 mM monovalent electrolyte. (*B*) Single-channel conductance at 200 mV (*X*) and −200 mV (□) plotted vs. concentration.

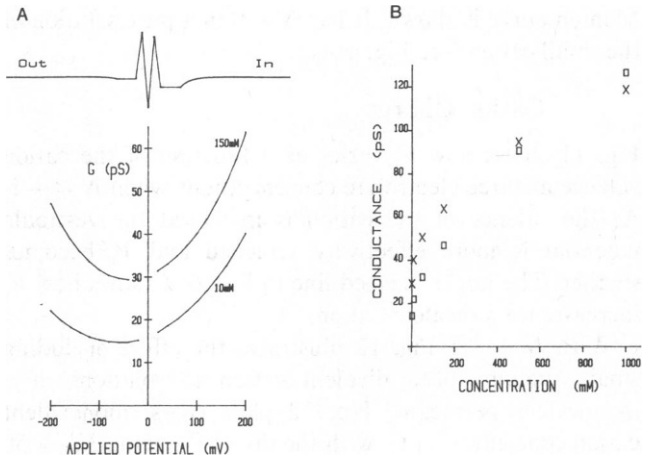

FIGURE 15 Shows asymmetric ion transport through a channel with each vestibule having a net charge of $N = -1$ but with binding only to the charge in the outer vestibule ($K_{do} = 50$ mM, $K_{di} = \infty$). (*A*) The energy profile calculated in 150 mM electrolyte has the final potential equal to −6 mV in the outer vestibule and −42 mV in the inner vestibule. Below, the single-channel conductance is plotted vs. the applied potential in 150 mM and 10 mM monovalent electrolyte. (*B*) Single-channel conductance at 200 mV (*X*) and −200 mV (□) plotted vs. concentration.

These two cases indicate that the vestibules may contribute to some biologically important cases of rectification due to such factors as size, shape, ion interactions, binding, the distribution of charge, and net charge.

SUMMARY AND CONCLUSION

The model presented here takes a simplified view of some physical properties of an ion channel. The vestibule at both ends of the channel is modeled as being in equilibrium with the bulk solution, possessing net-negative charge, and having a defined size and shape. Ion size, binding to the net charge in the vestibule, and blockage of current contribute to the vestibule's influence on ion transport. These features are coupled to a symmetrical two-barrier, one-site Eyring rate theory model that describes the narrow selective region of the pore. Any other more complicated barrier model could have been used.

It is likely that an ion experiences a progressive transition from bulk solution to intimate interaction with the amino acids in the pore. The separate treatment of the vestibule and the narrow region is artificial, especially since an ion probably senses some of the membrane potential in the vestibule, and restricted diffusion in this region may contribute to the relatively linear *I-V* relations often seen with biological channels. Properties displayed by the charged-vestibule model could equally result from distributed charges with a net charge in the narrow region. Some similar properties would occur even if the potential in the channel resulted from dipoles.

The properties explored in this paper suggest that concentration-dependent potentials in the channel and the size and shape of the vestibules can have many effects: (*a*) Wide vestibules reduce the length of the narrow region,

where the ion and channel must interact. By reducing this path of highest resistance, large vestibules enable channels to have larger maximum conductances (see Latorre and Miller, 1983 review). (*b*) The absolute value of the potential caused by net charge in the channel increases as the bulk electrolyte concentration decreases. This results because there is less screening of the net-negative charge in the pore. Thus, the vestibule potential is more effective at attracting cations. This produces conductances at low bulk concentrations that are larger than predicted from measurements at high concentrations. Rate theory models having multi-ion occupancy (Eisenman et al., 1978) or energy barriers that undergo time-dependent fluctuations (Eisenman and Dani, 1986) can also produce these relatively high conductances at low concentrations. (*c*) The potential inside the vestibule confers some cation vs. anion, and divalent vs. monovalent selectivity. A negative potential attracts divalent cations more strongly than monovalent cations, and it repells anions. The vestibule potential and its dependence on the electrolyte species in the bathing solution are strongly influenced by structural features that may have evolved to contribute to this general selectivity. Considerations of size, shape, and net charge may be particularly important in Ca channels. (*d*) Because of their size, large organic cations cannot enter the channel to screen the charged residues as well as small cations. Therefore, at an equivalent bulk concentration the cation-attracting potential in the vestibule is greater (more negative). This causes large cations to have a higher affinity for binding sites in the pore. Furthermore, when a very large cation enters the channel, it can displace some of the diffuse double layer thereby increasing the attractive potential due to the net charge in the channel. These factors, as well as hydrophobic interactions in the pore (Dywer et al., 1980; French and Shoukimas, 1985), may contribute to the relatively high affinity block of current by large impermeants such as TEA^+ and some local anesthetics. (*e*) The transport properties of a permeant can be altered by apparently insignificant changes in the ionic composition of the solution. Small amounts of a divalent, a large permeant, or a large impermeant all affect the apparent G_{max} and K_{site} of a permeant ion. This result suggests great caution must be exercised when changing the ionic environment bathing a channel even if the electrolyte is expected to be inert (see Oxford and Yeh, 1985). Furthermore, large applied potentials could alter the ionic composition interacting with the charge inside the pore: anions could be repelled, divalents attracted more than monovalents, and the permeant could be depleted in one vestibule and built-up in the other. This change in the diffuse, ionic layer would produce a different local potential in the channel, and in that way the energetics of transport may change when large potentials are applied to the membrane. (*f*) When the two entrances of a channel differ in size, shape, net charge, or ion binding, asymmetric transport characteristics can result.

I am grateful to M. Delay for many helpful interactions regarding the computer hardware and software, C. Clausen and D. Levitt for helpful discussions, B. Hille for commenting on the manuscript, and C. F. Stevens for providing equipment support (NS12961).

This work was supported by National Institutes of Health grant NS21229.

Received for publication 1985 and in final form 12 November 1985.

REFERENCES

Acton, F. S. 1970. Numerical methods that work. Harper and Row, NY. 541.

Apell, H.-J., E. Bamberg, H. Alpes, and P. Lauger. 1977. Formation of ion channels by a negatively charged analog of gramicidin A. *J. Membr. Biol.* 31:171–188.

Bash, P. A., R. Langridge, and R. M. Stroud. 1985. Model for the ion channel in the acetylcholine receptor. *Biophys. J.* 47(2, Pt. 2):43*a*. (Abstr.)

Brisson, A., and P. N. T. Unwin. 1985. Quaternary structure of the acetylcholine receptor. *Nature (Lond.)*. 315:474–477.

Cooper, K., E. Jakobsson, and P. Wolynes. 1985. The theory of ion transport through membrane channels. *Prog. Biophys. Molec. Biol.* 46:51–96.

Dani, J. A. 1985. Ionic interactions within the vestibules of ion channels. *Neurosci. Abstr.* 11:954.

Dwyer, T. M., D. J. Adams, and B. Hille. 1980. The permeability of the endplate channel to organic cations in frog muscle. *J. Gen. Physiol.* 75:469–492.

Eisenmann, G., and J. A. Dani. 1986. Characterizing the electrical behavior of an open channel via the energy profile for ion permeation—a prototype using a fluctuating barrier model for the acetylcholine receptor channel. *In* Proceedings, International School on Ionic Channels. Santiago, Chile. In press.

Eisenman, G., J. A. Dani, and J. Sandblom. 1985. Recent studies on the energy profiles underlying permeation and ion selectivity of the gramicidin and acetylcholine receptor channels. *In* Recent Advances in the Theory and Application of Ion Selective Electrodes in Physiology and Medicine. M. Kessler, D. K. Harrison, and J. Hoper, editors. Springer-Verlag, Berlin-Heidelberg-New York.

Eisenman, G., J. Sandblom, and E. Neher. 1978. Interactions in cation permeation through the gramicidin channel: Cs, Rb, K, Na, Li, Tl, H, and. effects of anion binding. *Biophys. J.* 22:307–340.

Finer-Moore, J., and R. M. Stroud. 1984. Amphipathic analysis and possible formation of the ion channel in an acetylcholine receptor. *Proc. Natl. Acad.Sci. USA.* 81:155–159.

Fischer, W., J. Brickmann, and P. Lauger. 1981. Molecular dynamics study of ion transport in transmembrane protein channels. *Biophysical Chem.* 13:105–116.

Frehland, E. 1979. Thery of transport noise in membrane channels with open-closed kinetics. *Biophys. Struct. Mechanism.* 5:91–106.

French, R. J., and J. J. Shoukimas. 1985. An ion's view of the potassium channel: the structure of the permeation pathway as sensed by a variety of blocking ions. *J. Gen. Physiol.* 85:669–698.

Gates, P., and E. Jakobsson. 1985. Brownian dynamic simulations of ion movement in a gramicidin-like channel. *Biophys. J.* 47(2, Pt. 2):432*a*. (Abstr.)

Gilbert, D. L., and G. Ehrenstein. 1969. Effect of divalent cations on potassium conductance of squid axons: determination of surface charge. *Biophys. J.* 9:447–463.

Grahame, D. C. 1947. The electrical double layer and the theory of electro-capillarity. *Chem. Rev.* 41:441–501.

Guy, H. R. 1984. A structural model of the acetylcholine receptor channel based on partition energy and helix packing calculations. *Biophys. J.* 45:249–261.

Hagglund, J. V., G. Eisenman, and J. P. Sandblom. 1984. Single-salt

behavior of a symmetrical 4-site channel with barriers at its middle and ends. *Bull. Math. Biol.* 46:41–80.

Hille, B. 1984. Ionic Channels in Excitable Membranes. Sinauer Associates, Sunderland, MA. 426.

Hille, B., A. M. Woodhull, and B. I. Shapiro. 1975. Negative surface charge near sodium channels of nerve: divalent ions, monovalent ions, and pH. *Phil. Trans. R. Soc. Lond.* 270:301–318.

Hodgkin, A. L., and A. F. Huxley. 1952. A quantitative description of membrane current and its application to conduction and excitation in nerve. *J. Physiol. (Lond.).* 117:500–544.

Huang, L. M., W. A. Catterall, and G. Ehrenstein. 1978. Selectivity of cations and nonelectrolytes for acetylcholine-activated channels in cultured muscle cells. *J. Gen. Physiol.* 71:397–410.

Jordan, P. C. 1984. The total electrostatic potential in a gramicidin channel. *J. Membr. Biol.* 78:91–102.

Kistler, J., R. M. Stroud, M. W. Klymkowsky, R. A. Lalancette, and R. H.. Fairclough. 1982. Structure and function of an acetylcholine receptor. *Biophys. J.* 37:371–383.

Latorre, R., and C. Miller. 1983. Conduction and selectivity in potassium channels. *J. Membr. Biol.* 71:11–30.

Lauger, P., W. Stephan, and E. Frehland. 1980. Fluctuations of barrier structure in ionic channels. *Biochim. Biophys. Acta.* 602:167–180.

Lee, W. K., and P. C. Jordan. 1984. Molecular dynamics simulation of cation motion in water-filled gramicidinlike pores. *Biophys. J.* 46:805-819.

Levitt, D. G. 1982. Comparison of Nernst-Planck and reaction-rate models for multiply occupied channels. *Biophys. J.* 37:575–587.

Levitt, D. G. 1985. Strong electrolyte continuum theory solution for equilibrium profiles, diffusion limitation, and conductance in charged ion channels. *Biophys. J.* 48:19–31.

Lewis, C. A., and C. F. Stevens. 1979. Mechanism of ion permeation through channels in a postsynaptic membrane. *In* Membrane Transport Processes. C. F. Stevens and R. W. Tsien, editors. Raven Press, NY. 3:133–151.

Mackay, D. H. J., P. H. Berens, K. R. Wilson, and A. T. Hagler. 1984. Structure and dynamics of ion transport through gramicidin A. *Biophys. J.* 46:229–248.

McLaughlin, S. 1977. Electrostatic potentials at membrane-solution interfaces. *Curr. Top. Membr. Transp.* 9:71–144.

McLaughlin, S., G. Szabo, and G. Eisenman. 1971. Divalent ions and surface potential of charged phospholipid membranes. *J. Gen. Physiol.* 58:667–687.

Maeno, T., C. Edwards, and M. Anraku. 1977. Permeability of the end-plate membrane activated by acetylcholine to some organic cations. *J. Neurobiol.* 8:173–184.

Mishina, M., T. Tobimatsu, K. Imoto, K. Tanaka, Y. Fujita, K. Fukuda, M. Kurasaki, H. Takahashi, Y. Morimoto, T. Hirose, S. Inayama, T. Takahashi, M. Kuno, and S. Numa. 1985. Location of functional regions of acetylcholine receptor alpha-subunit by site-directed mutagenesis. *Nature (Lond.).* 313:364–369.

Noda, M., S. Shimizu, T. Tanabe, T. Takai, T. Kayano, T. Ikeda, H. Takahashi, H. Nakayama, Y. Kanaoka, N. Minamino, K. Kangawa, H. Matsuo, M.A. Raftery, T. Hirose, S. Inayama, H. Hayashida, T. Miyata, and S. Numa. 1984. Primary structure of *Electrophorus electricus* sodium channel deduced from cDNA sequence. *Nature (Lond.).* 312:121–127.

Noda, M., H. Takahashi, T. Tanabe, M. Toyosato, S. Kikyotani, Y. Furutani, T. Hirose, H. Takashima, S. Inayama, T. Miyata, and S. Numa. 1983. Structural homology of *Torpedo californica* acetylcholine receptor subunits. *Nature (Lond.).* 302:528–532.

Oxford, G. S., and J. Z. Yeh. 1985. Interactions of monovalent cations with sodium channels in squid axon. I. Modification of physiological inactivation gating. *J. Gen. Physiol.* 85:583–602.

Sakmann, B., and E. Neher, editors. 1983. Single-channel recording. Plenum Publishing Corp., NY. 503.

Sanchez, J. A., J. A. Dani, D. Siemen, and B. Hille. 1986. Slow permeation of organic cations in acetylcholine receptor channels. *J. Gen. Physiol.* In press.

Young, E. F., E. Ralston, J. Blake, F. Ramachandran, Z. W. Hall, and R. M. Stroud. 1985. Topological mapping of acetylcholine receptor: evidence for a model with five transmembrane segments and a cytoplasmic COOH-terminal peptide. *Proc. Natl. Acad. Sci. USA.* 82:626–630.

White, M. M., K. M. Mayne, H. A. Lester, and N. Davidson. 1985. Mouse-*Torpedo* hybrid acetylcholine receptors: functional homology does not equal sequence homology. *Proc. Natl. Acad. Sci. USA.* 82:4852–4856.